Sirte University Scientific Journal(Applied Sciences) Vol.7(2),76–97,December2017

Modeling of Bifurcation and Post-Bifurcation Response of Granular Materials: Insights From Discrete Element Modeling

Abdalsalam M. Muftah[1] and Marte Gutierrez[2]*
e-mail: salamgader@su.edu.ly

[1]*Sirte University/Faculty of Engineering (SU), Libya*
[2]*Colorado School of Mines/Division of Engineering (CSM), USA*

Abstract

A softening elastoplasticity model for sand has been constructed and its mathematical derivations are described in this paper. The proposed model is based on the concept of a non-associated elastoplastic material description. The model first was coupled with a strain hardening plasticity model, as developed by Gutierrez 2010 [1], for granular soil before the bifurcation point. The softening elastoplasticity model then develops a tangential stiffness matrix which plays a crucial role in describing the softening behavior. The smeared shear band model proposed by Pietruszczak and Mroz 1981 [2] is employed in this model to incorporate a characteristic length dimension (i.e. shear band thickness). The objectivity of the constitutive model has been established from the form-invariance principal. The plastic module in terms of stress and strain-increments is provided for simulating stress and strain-controlled biaxial tests. The results of a study of RF-Huston sand and of DEM simulation served as a basis for evaluating the capabilities of the model. The results indicate that, the softening elastoplasticity model accurately depicts the trends observed in the experimental data of RF-Hostun and the DEM sand simulation.

Keywords:*hardening plasticity, smeared shear band, StrainLocalization, non-associated flow rule, Prager's consistency condition, Noncoaxiality, Stress rotations*

1. Introduction

When a granular structure is subjected to external loading, various stress or strain states occur in the structure. A typical deviatoric stress-axial strain behavior of frictional granular soil under triaxial compression condition, for example, usually consists of both strain hardening and softening portions. Soil shear strength increases (hardens) initially and then decreases (softens) after the deviatoric stress reaches a peak value or a bifurcation point. The development of softening continues until residual state is reached (Fig. 1). The soil hardening and softening

behaviors are modeled by an isotropic increase and decrease of yield surface which is governed by different theories as the elastoplasticity.

The topic of strain-softening has recently attracted extensive research because efforts to model the failure of granular soils are inevitably linked with stress-strain curves. The earliest such work focused on the stability of earth structures due to the importance of strain softening in these systems [3,4,5,6,7]. A number of works have been published recently, which focus on various aspects of strain softening analysis considering stability of bifurcation for granular soil materials. [8,9,10]. The post localization model describes the strain softening response that follows the onset of strain localization. In these cases, strain softening is usually beyond the bifurcation point in which the material develops large strain that eventually lead to failure. In the post localization regime we deal in general with the most difficult aspect of granular behavior and mathematical challenges in modeling the post localization phase. This complexity of behavior can be interpreted due to the formation of a shear band. Once the shear band is formed, the constitutive response of the particulate system is dominated by what happens inside the band. The mechanical response of the shear band affects the response of intact systems during continued increase in deformation [7,11].

Softening in terms of elastoplasticity theory means a contraction of the yield surface as a result of which the loading surface softens (decreases in size). The totality of plastic states bounding the elastic range, defines a yield surface. The elastic stress increments are related to strain increments by Hook's law (Eq. 9). Plastic stress increments can be determined by the corresponding plastic strain increments by updating the loading condition. In this scenario, the loading from one plastic state leads to another plastic state on the stress path. This condition is called the consistency condition [12,13].

Numerous numerical studies have been performed to simulate the post localization regime. In the mathematical sense, the cause of these problems is the fact that the partial differential equation changes type in the transition from hardening to softening, so that the boundary value becomes imaginary [14,15]. Finite element simulation of post localization response has a number of limitations such as the predicted load carrying capacity exhibits strong mesh dependency, and the shear band thickness approaches zero as the mesh is continuously refined [2,16]. These results are in contradiction with experimental data, which indicate a finite width for the localization zone. Strain softening effects are also often observed in conventional laboratory biaxial tests for a dense granular material[17,19]. After a stress state reaches the peak surface, the response of stress-strain switches from a hardening relation to a softening state. Such softening involves a reduction of the friction angle and increase of plastic work which causes the deflation of the yield surface. In enhanced continuum theory, including Casseret continuum theory, gradient plasticity and non-

local constitutive models have been proposed to introduce a length scale into the constitutive relation to define the microstructure of material undergoing inhomogeneous deformation [16,20]. The objective of this part of the study is to investigate the post localization response of dilatants on the granular system without routing those difficult approaches which use enhanced continuum theories. This approach assumes that once the shear band is formed, all deformation occurs inside the shear band. It assumed that elastic deformations inside the shear band are negligible as compared to plastic deformations. The strain softening behavior, which is accompanied by localization of deformation inside the shear band, does not represent a characteristic of material element, since the homogeneity of strain is lost with the onset of shear hardening. The loading function for such a material will in general decrease in size with further straining.

This study focuses on softening elastoplasticity models enhanced by incremental formulation of internal variables, such as friction and dilatancy angles. The aim of this study is to find an elastoplasticity model for strain softening materials that acts as a localization descriptor, both for localization due to softening and due to non-associated plastic flow. We are more interested in the strain softening inside the shear band. Softening was accompanied by shear banding in the majority of the biaxial compression tests. The occurrence of banding softening, instead of material softening was reported by [10]. Wanatowski et al. state that strain softening inside the shear band is crucial for the development of a shear band system. A number of different mechanisms can be responsible for decreases in shear strength at soil when granular soil reaches peak strength, for example, negative stress increments may develop and its strength drops down to some limiting or residual value. The phenomenon when stress decreases with an increase in strain is generally called “strain softening”, during which a main characteristic is that the tangent modulus becomes negative [2,21]. During plastic loading in the softening region, the stresses decreases in value causing contraction of the stress yield surface.

In this paper, two different model components are discussed in order to construct a softening elastoplasticity model. The first component is a hardening plasticity model [1] for simulating the granular soil behavior prior to reaching the bifurcation point. As soon as the bifurcation point is reached the hardening model is replaced by a softening model. The second component is an elastic-plastic constitutive model with strain softening to simulate the strain softening behavior beyond the bifurcation point. The later component is in the form of the so-called smeared shear band [2].

2. Review of Hardening Plasticity Model

For strain hardening material, the yield surface must change in some way so that an increase in stress is necessary to induce further plastic deformation. Several hardening rules have been proposed in the past for use in plastic analysis. A complete strain hardening model based on

simple constitutive formulation of the response of the sand is constructed [1]. The elastoplastic constitutive model for a biaxial loading condition is introduced, which adequately captures the monotonic response of granular soils until the bifurcation point is reached, particularly the variation of the mobilized friction and the dilatancy with shear deformation. This model has the following components:

1. The yielding function $f(s,t,\emptyset)$ in spirit of the Mohr-coulomb yield criterion given by $f = t + ssin\emptyset$ and $sin\emptyset$ as the hardening parameter.

2. The friction and dilation angles in granular soil are varies with shear deformation. The strain hardening function is based on a hyperbolic relation between $sin\emptyset$ and plastic strainγ^p. The plastic potential function $g(s,t,\varphi)$is derived from the stress-dilatancy relation.

3. Elastic shear strain can be calculated using the value of Poisson's ratio ν and the shear modulus.

Based on these definitions, the hardening parameter h can be derived

$$h = \frac{ssin\emptyset_p}{A}(1 - \frac{sin\emptyset}{sin\emptyset_p})^2 \qquad (1)$$

The friction angle $sin\emptyset_B$ and the corresponding shear strain γ_B at the point of bifurcation are obtained in this model

$$sin\emptyset_B = sin\emptyset_p(1 - sin\emptyset_c\sqrt{\frac{1}{8(1-\nu)S_B}\frac{G}{G_B}})\gamma_B = \frac{Asin\emptyset_B}{sin\emptyset_p - sin\emptyset_B} \qquad (2)$$

The constitutive model predictions are compared against experimental data. The demonstration is performed for two densities (loose and dense) of RF-Hostun sand. Data for RF-Hostun sand was used to compare the stress-strain response of experimental biaxial tests with the response of the constitutive model until the bifurcation point achieved. The results for loose and dense RF-Hostun sand were first performed isotropically consolidation at initial mean stress of S_o=100, 200, 400 and 800KPa. The samples were then sheared under σ_3-constant condition. The model and experimental results show good agreement and consistency until the bifurcation point is reached. After the bifurcation point, the predicted stress-strain curve, which assumes homogenous response, continues to show strain hardening and then deviates from the experimental data, which show strain softening. The predicted volumetric vs. shear strain curves also start to deviate from the experimental data after the bifurcation point. The plane strain biaxial test results for dense RF-Hostun sands and the response using the constitutive model are shown in Fig. 2.

When the bifurcation point reached, the constitutive model for biaxial loading condition before bifurcation is no longer applicable. A precise elastoplastic constitutive model is required, which adequately captures the strain-softening response of granular materials particularly the variation of dilatancy and mobilized friction with shear deformation. In the next section, the incremental constitutive stiffness matrix for a granular assembly is derived by employing internal variables such as the thickness and the shear band, friction and dilatancy angles. The hardening model is based on the concept of elastoplasticity. As previously approached for granular soils by [1], the model will be extended to include a non-associated elastic-plastic constitutive model with strain softening to describe the granular soil behavior beyond the bifurcation point.

3. Review of the Smeared Shear Band Model

Many published papers have focused on various aspects of strain softening analysis, and many experiments have been carried out on granular sand materials with efforts to clarify the relationships between the strain softening behavior of sand and the formation of the shear band. It appears that the model of [2] has the greatest potential for studying problem post-localization, since it incorporates both material and geometrical components of strain softening phenomena. Pietruszczak and Mroz[2]developed a model of localized failure with finite element for granular soil, in which the plastic shear deformations are smeared within a band across the element (Fig. 3). It is assumed a priori that the band has thickness d and the shear band angle α is oriented relative to the direction of major principal stress. The behavior of a non-cohesive material with associated flow rule was considered in their original work. Pietruszczak and Mroz[2]indicate that the model overcomes the problem of mesh sensitivity associated with the more conventional strain softening finite element analysis. No assessment of bifurcation is made and it is assumed that localization occurs when stresses reach the yield surface.

The smeared shear band model takes into account the effect of a characteristic smeared band length, the shear band thickness, and the geometry of the specimen when evaluating the response of strain softening. Following the Pietruszczak and Mroz model, shear banding is introduced in the numerical model by a strain localization parameter η in the additive decomposition of total strain increment $d\varepsilon$ into two parts in series as shown in Fig. 3, one referring to elastic $(d\varepsilon^e)$ part outside shear band and one referring to plastic $(d\varepsilon^p)$ parts inside shear band as follow

$$d\varepsilon = d\varepsilon^e + \eta\, d\varepsilon^p \qquad (3)$$

where

$$\eta = \frac{Theareaofshearband\ (F_w)}{Theareaoftheelement\ (F_e)} \quad (4)$$

$$\eta = \frac{Shear\ band\ thickness\ (d)}{The\ hight\ of\ the\ element\ (a) \times cos\ (\propto)} \quad (5)$$

The length scaling constant η is a function of element size and since shear band thickness is treated as constant, a linear reduction in element size leads to a linear increase in η. The length scaling factor η represents the geometric component of strain softening and acts to adjust the amount of strain softening. The constitutive relation in the form of the stress-strain relationship reported by [2]was obtained as.

$$\sigma = [T]\left\{\frac{F_w}{F_e}\frac{1}{H}[C] + \frac{1}{E}[D]\right\}^{-1}[T](\varepsilon) \quad (6)$$

where H represents the softening modulus of the shear band material, and $[T]$ represents the transformation matrix. The value $[c]$ represents the plastic stiffness matrix and is defined as:

$$C_{ij} = \frac{df}{d\sigma_i}\frac{df}{d\sigma_j} \quad (7)$$

In the next section, the incremental constitutive stiffness matrix for the element is derived by considering the shear band to penetrate through a constant strain element. In the proposed model we advocate the concept put forward in [2], which takes into account the incorporation of a characteristic dimension, such as the width of the shear band and the geometry of the specimen into the constitutive relation.

4. Model Description

Elastoplasticity method is a phenomenological method. Its aim is to produce mathematically the macroscopic relation between stress and strain tensor in a material point of the body for different loading conditions. Such a mathematical description is commonly named a constitutive model. The constitutive model developed here will be based on an elastoplasticity framework. A fundamental notion in the elastoplasticity theory is the existence of a yield function that bounds the elastic domain.To set up an elastoplasticity model, the proposed model is coupled with a strain hardening model as developed by [1]. The yield function f and plastic potential function g are of Mohr-coulomb type. The smeared shear band method proposed in the Pietruszczak and Mroz model [2]is employed to incorporate the characteristic length scale of strain localization.

The material is initially homogenously distributed over the sample in the post localization model. All boundaries of the biaxial test are smooth. The top plate and base plate of the biaxial setup can move independently in a horizontal direction. The post-localization model describes the biaxial test in two areas, one inside and one outside of the shear band. The material outside of the shear band is assumed to react to the applied stress in an elastic manner. The material inside of the shear band behaves plastically. The shear band has thickness d and is inclined at an angle α to the x-axis. It is assumed that only one shear band will develop during the biaxial tests. The stress components along the shear band follow the rotation of the axis with angle. The material properties and the material outside and inside shear band can be different. The parameters outside the band have the superscript e (elastic). The parameters inside the band have the superscript p (plastic) (see Fig. 4).

5. Formulation of the Elastic-Plastic Constitutive Model

Following the solutions proposed by Pietruszczak and Mroz model, this method takes into account strain localization associated with shear banding by introducing a characteristic length scale η and by defining shear deformation characteristics inside shear band. These shear deformation characteristics are obtained by the decomposition of the total strain ε into an elastic, reversible part, ε^e and a plastic, irreversible part, ε^p

$$\varepsilon = \varepsilon^e + \eta\, \varepsilon^p \qquad (8)$$

If considered in terms of incremental strains, the total strain increment is obtained from the expression in Eq. 3.

The elastic strain increment is linearly related to the stress increment $d\sigma$

$$d\sigma = E d\varepsilon^e \qquad (9)$$

The plastic flow within a shear band is formulated in the spirit of the Mohr-Coulomb elastoplasticity model with a non-associated flow rule. The plastic strain herein can be represented by assuming the yield function f and plastic potential function g as:

$$f = \tau_{nt} + \sigma_n tan\phi \;\text{ and, }\; g = \tau_{nt} + \sigma_n tan\varphi \qquad (10)$$

where τ_{nt} and σ_n represent the shear stress and normal stress which are usually calculated at the onset of bifurcation to understand the initiation of strain localization.

In theory, a spectral analysis can be performed at any loading steps past the initial bifurcation point. These post bifurcation analyses, which are difficult to interpret due to heterogeneous modes of deformations, are beyond the scope of this paper. Inside the shear band, the stress and strain components are formulated along the $n\ and\ t$ axis. In two dimensions, the shear stress τ_{nt} and normal stress σ_n can be written in terms of the two-dimensional MIT stress invariants p and q, which are equal to the coordinate of the center and the radius of Mohr's circle of stress, respectively (Fig. 5):

$$\tau_{nt} = -q\sin(2\alpha) \tag{11}$$

$$\sigma_n = p + q\cos(2\alpha) \tag{12}$$

$$p = \frac{1}{2}(\sigma_1 + \sigma_3)\ \ and\ \ q = \frac{1}{2}(\sigma_1 - \sigma_3) \tag{13}$$

where $\sigma_1$the major principal is stress and σ_3 is the minor principal stress (compression being taken as positive sign). Accordingly, the Mohr-Coulomb criterion for yield stress f, and plastic potential g become:

$$f = -\frac{1}{2}(\sigma_1 - \sigma_3)\sin(2\alpha) + \left(\frac{1}{2}(\sigma_1 + \sigma_3) + \frac{1}{2}(\sigma_1 - \sigma_3)\cos(2\alpha)\right)\tan(\emptyset) \tag{14}$$

$$g = -\frac{1}{2}(\sigma_1 - \sigma_3)\sin(2\alpha) + \left(\frac{1}{2}(\sigma_1 + \sigma_3) + \frac{1}{2}(\sigma_1 - \sigma_3)\cos(2\alpha)\right)\tan(\varphi) \tag{15}$$

However, unlike the Pietruszczak and Mroz model, the variation of the mobilized friction angle$\emptyset$ and dilatancy angleφ are specified in the present study. Also, it is assumed non-associated flow, which requires that f and g do not coincide.

For simplicity, a strain softening function exhibits approximately linear relation between mobilized function angle $\tan\emptyset$ and plastic shear strain γ_{13}^{p}, and is most commonly used to define a softening model. The value of B is equal to the initial slope of $\tan\emptyset$vs. $\gamma_{13}^{p}$and its value is always positive. So the constitutive relation for granular soils in the strain softening stage can be considered as a descending straight line whose absolute value of the slope is$B$, the shear softening modulus.

$$\tan\emptyset = B\gamma_{13}^{p} \tag{16}$$

According to the theory of plasticity, the plastic strain increments are proportional to the derivative of the plastic potential function g with respect to the stresses. The increment of plastic strain $d\varepsilon_{ij}^{p}$ for the entire assembly is

$$d\varepsilon_{ij}^{p} = \lambda \frac{dg}{d\sigma_{ij}} \tag{17}$$

The principal strain increments $d\varepsilon_{1}^{p}, d\varepsilon_{3}^{p}$ and the shear strain increment $d\gamma_{13}^{p}$can be determined from Eq. 17

$$d\varepsilon_{1}^{p} = \lambda \frac{dg}{d\sigma_{1}} \ , \ \ d\gamma_{13}^{p} = \lambda \frac{dg}{d\tau} \ \ and \ \ d\varepsilon_{3}^{p} = \lambda \frac{dg}{d\sigma_{3}} \tag{18}$$

In which λ is the rate form of the so-called plastic multiplier. This is just a multiplier that does not have a direct physical meaning. In the case of purely elastic behavior λ is zero whereas in the case of plastic behavior λ is positive and dg is the increment of plastic potential function. The value of λ can be evaluated by invoking the so-called Prager's consistency condition for plastic flow, which reflects the principal that a material point remains in plastic state ($df = 0$, where f is the yield function).

The evolution of the yield function can be obtained as:

$$df = \frac{df}{d\sigma_{1}} d\sigma_{1} + \frac{df}{d\sigma_{3}} d\sigma_{3} + \frac{df}{d\tan\emptyset} d\tan\emptyset = 0 \tag{19}$$

The yield function is expressed in terms of stress invariants. The derivatives of the yield function with regards to stresses may be obtained for each derivative term through the chain rule:

$$\frac{df}{d\sigma_{1}} = \frac{df}{d\tau}\frac{d\tau}{d\sigma_{1}} + \frac{df}{d\sigma_{n}}\frac{d\sigma_{n}}{d\sigma_{1}} and \frac{df}{d\sigma_{3}} = \frac{df}{d\tau}\frac{d\tau}{d\sigma_{3}} + \frac{df}{d\sigma_{n}}\frac{d\sigma_{n}}{d\sigma_{3}} \tag{20}$$

The derivatives of yield function with respect to the stress invariants are derived from Eq. 10:

$$\frac{df}{d\tau} = 1 \ and \ \ \frac{df}{d\sigma_{n}} = \tan\emptyset \tag{21}$$

and the derivatives of the stress invariants with respect to general state of stresses are derived from Eqs. 11 and 12:

$$\frac{d\tau}{d\sigma_1} = -\frac{1}{2}sin2\alpha, \qquad \frac{d\sigma_n}{d\sigma_1} = \frac{1}{2}(1 + cos2\alpha), \qquad \frac{d\sigma_n}{d\sigma_3} = \frac{1}{2}(1 - cos2\alpha) \; and \; \frac{d\tau}{d\sigma_3} = \frac{1}{2}sin2\alpha \qquad (22)$$

Substituting these values in Eq. (20), one obtains

$$\frac{df}{d\sigma_1} = -\frac{1}{2}sin2\alpha + \frac{1}{2}(1 + cos2\alpha)\tan\emptyset \; and \; \frac{df}{d\sigma_3} = \frac{1}{2}sin2\alpha + \frac{1}{2}(1 - cos2\alpha)\tan\emptyset \quad (23)$$

A similar expression can be derived for the derivatives of plastic potential functions in terms of stress invariants and with respect to general state of stresses, using the chain rule.

$$\frac{dg}{d\sigma_1} = \frac{dg}{d\tau}\frac{d\tau}{d\sigma_1} + \frac{dg}{d\sigma_n}\frac{d\sigma_n}{d\sigma_1} and \frac{df}{d\sigma_3} = \frac{dg}{d\tau}\frac{d\tau}{d\sigma_3} + \frac{dg}{d\sigma_n}\frac{d\sigma_n}{d\sigma_3} \qquad (24)$$

The derivatives of yield function with respect to the stress invariants are derived from Eq. 10:

$$\frac{dg}{d\tau} = 1 \; and \; \frac{dg}{d\sigma_n} = \tan\varphi \qquad (25)$$

Substituting these values in Eq. 24, one obtain

$$\frac{dg}{d\sigma_1} = -\frac{1}{2}sin2\alpha + \frac{1}{2}(1 + cos2\alpha)\tan\varphi \; and \; \frac{dg}{d\sigma_3} = \frac{1}{2}sin2\alpha + \frac{1}{2}(1 - cos2\alpha)\tan\varphi \qquad (26)$$

Equation 16 can be differentiated as follows to obtain

$$dtan\emptyset = Bd\gamma_{13}^{p} \qquad (27)$$

In this model, the local plastic shear strain $d\gamma_{13}^{p}$ is characterized by Eq.18. The incremental mobilized friction angle can be obtained as follows

$$dtan\phi = B\lambda\frac{dg}{d\tau} \qquad (28)$$

The derivatives of the yield function with regard to the mobilized friction angle may be obtained as:

$$\frac{df}{dtan\phi} = \sigma_n \qquad (29)$$

The implementation of the softening constitutive model requires an incremental form in which the stress increments $d\sigma_1$are expressed in terms of the total strain increments $d\varepsilon_1$ and the plastic strain increment $d\varepsilon_1^p$, as follows

$$d\sigma_1 = E\left(d\varepsilon_1 - \eta d\varepsilon_1^p\right) \tag{30}$$

During plastic flow, the stress tensor increment $d\sigma_1$can be related to both the strain and local yields strength increment $d\varepsilon_1$ and $\frac{dg}{d\sigma_1}$ respectively.

$$d\sigma_1 = E\left(d\varepsilon_1 - \eta\lambda\frac{dg}{d\sigma_1}\right) \tag{31}$$

where E is the elastic modulus tensor. After some arrangement in terms of ε_{ij} and λ, the following equation can be obtained

$$\frac{df}{d\sigma_1}E\left(d\varepsilon_1 - \eta\lambda\frac{dg}{d\sigma_1}\right) + \frac{df}{d\sigma_3}d\sigma_3 + \frac{df}{d\tan\emptyset}d\tan\emptyset = 0$$

$$\frac{df}{d\sigma_1}Ed\varepsilon_1 - \eta\lambda E\frac{df}{d\sigma_1}\frac{dg}{d\sigma_1} + \frac{df}{d\sigma_3}d\sigma_3 + \lambda B\sigma_n\frac{dg}{d\tau} = 0$$

$$\lambda\left(\eta E\frac{df}{d\sigma_1}\frac{dg}{d\sigma_1} - B\sigma_n\frac{dg}{d\tau}\right) = \frac{df}{d\sigma_1}Ed\varepsilon_1 + \frac{df}{d\sigma_3}d\sigma_3$$

Thus, the positive plastic multiplier λ can be expressed as

$$\lambda = \frac{\frac{df}{d\sigma_1}Ed\varepsilon_1 + \frac{df}{d\sigma_3}d\sigma_3}{\left(\eta E\frac{df}{d\sigma_1}\frac{dg}{d\sigma_1} - H_p\right)} \tag{32}$$

where $H_p$is defined as a plastic modulus

$$H_p = B\sigma_n\frac{dg}{d\tau} \tag{33}$$

Geotechnical tests are partly stress and partly strain controlled. For instance, a biaxial test is conducted by controlling the vertical principal strain rate and a horizontal stress. Suppose now we

partially control the principal major stress $\sigma_1$and partially control the principal minor strainε_3. Then, substituting Eq. 32 into Eq. 31, one can obtain the equation as:

$$d\sigma_1 = E\left(d\varepsilon_1 - \eta\frac{E\frac{df}{d\sigma_1}\frac{dg}{d\sigma_1}d\varepsilon_1 + \frac{df}{d\sigma_3}\frac{dg}{d\sigma_1}d\sigma_3}{\left(\eta E\frac{df}{d\sigma_1}\frac{dg}{d\sigma_1} - H_p\right)}\right) \tag{34}$$

This implementation also requires an incremental strain form $d\varepsilon_3$which is expressed in terms of the total strain increment $d\varepsilon_1$ and the incremental minor stress $d\sigma_3$as follows:

$$d\varepsilon_3 = \frac{d\sigma_3}{G} + \lambda\frac{dg}{d\sigma_3} \tag{35}$$

$$d\varepsilon_3 = \frac{d\sigma_3}{G} + \eta\frac{E\frac{df}{d\sigma_1}\frac{dg}{d\sigma_3}d\varepsilon_1 + \frac{df}{d\sigma_3}\frac{dg}{d\sigma_3}d\sigma_3}{\left(\eta E\frac{df}{d\sigma_1}\frac{dg}{d\sigma_1} - H_p\right)} \tag{36}$$

The plastic flow rule for the entire assembly in Eqs. 34 and 36 can be written in the matrix form:

$$\begin{Bmatrix} d\sigma_1 \\ \\ d\varepsilon_3 \end{Bmatrix} = \begin{bmatrix} E\left(1 - \frac{E\eta\frac{df}{d\sigma_1}\frac{dg}{d\sigma_1}}{\left(\eta E\frac{df}{d\sigma_1}\frac{dg}{d\sigma_1} - H_p\right)}\right) & \frac{-E\eta\frac{df}{d\sigma_3}\frac{dg}{d\sigma_1}}{\left(\eta E\frac{df}{d\sigma_1}\frac{dg}{d\sigma_1} - H_p\right)} \\ \frac{E\eta\frac{df}{d\sigma_1}\frac{dg}{d\sigma_3}}{\left(\eta E\frac{df}{d\sigma_1}\frac{dg}{d\sigma_1} - H_p\right)} & \frac{1}{G} + \frac{E\eta\frac{df}{d\sigma_3}\frac{dg}{d\sigma_3}}{\left(\eta E\frac{df}{d\sigma_1}\frac{dg}{d\sigma_1} - H_p\right)} \end{bmatrix} \begin{Bmatrix} d\varepsilon_1 \\ \\ d\sigma_3 \end{Bmatrix} \tag{37}$$

$$\begin{Bmatrix} d\sigma_1 \\ d\varepsilon_3 \end{Bmatrix} = \begin{bmatrix} D_{11} & D_{12} \\ D_{21} & D_{22} \end{bmatrix} \begin{Bmatrix} d\varepsilon_1 \\ d\sigma_3 \end{Bmatrix} \tag{38}$$

Thus, the elasto-plastic constitutive relationship under a biaxial loading test is presented by using the elasto-plastic theory in strain space and taking compression in $d\sigma_1$ as positive loading. The confining pressure or side loading is a constant load ($d\sigma_3 = 0$), as established in the DEM and the experimental tests. With these results in hand, we can further refine the incremental form of the stress-strain constitutive equation. The constitutive model in the flow theory of plasticity gives the stress increment in terms of the strain increment:

$$d\sigma_1 = [D_{11}\,]d\varepsilon_1 \qquad d\sigma_1 = \left[E\left(1 - \frac{E\eta\frac{df}{d\sigma_1}\frac{dg}{d\sigma_1}}{\left(\eta E\frac{df}{d\sigma_1}\frac{dg}{d\sigma_1} - H_p\right)}\right)\right]d\varepsilon_1 \qquad (39)$$

$$d\varepsilon_3 = [D_{21}\,]d\varepsilon_1 \qquad d\varepsilon_3 = \left[\frac{E\eta\frac{df}{d\sigma_1}\frac{dg}{d\sigma_3}}{\left(\eta E\frac{df}{d\sigma_1}\frac{dg}{d\sigma_1} - H_p\right)}\right]d\varepsilon_1 \qquad (40)$$

Substituting the expression Eqs: 23, 25 and 26 into equation 39 and 40

$$d\sigma_1 = \left[E\left(1 - \frac{\frac{E}{4}\eta(sin2\alpha - (1+cos2\alpha)\tan\emptyset)(sin2\alpha - (1+cos2\alpha)\tan\varphi)}{\left(\frac{E}{4}\eta(sin2\alpha - (1+cos2\alpha)\tan\emptyset)(sin2\alpha - (1+cos2\alpha)\tan\varphi) - B\sigma_n\right)}\right)\right]d\varepsilon_1 \qquad (41)$$

$$d\varepsilon_3 = \left[\frac{\frac{E}{4}\eta(sin2\alpha - (1+cos2\alpha)\tan\emptyset)(sin2\alpha - (1+cos2\alpha)\tan\varphi)}{\left(\frac{E}{4}\eta(sin2\alpha - (1+cos2\alpha)\tan\emptyset)(sin2\alpha - (1+cos2\alpha)\tan\varphi) - B\sigma_n\right)}\right]d\varepsilon_1 \qquad (42)$$

The internal variables in these functions can be used in order to address elasto-plasticity softening features. The effects of parameters on the shape and the size of yield surfaces are clearly demonstrated and illustrated for all function in biaxial strain space. The aim of this study is to present such constitutive formulation and to test the method on a fairly simple example that was studied previously using a discrete element method approach, and using previously experimental data on loose and dense RF-Hostum sand. In this study, we assume development of a shear band during softening and derive effective stiffness matrices accounting for their effect, but the incremental analysis is carried out in the usual way without separate treatment of the shear band and the surrounding material.

The input file in the present model is built up on the following information: (1) Input the most basic material properties, such as the modulus of elasticity E, passion's ratio υ, internal friction angle ϕ and dilation angle φ; (2) Input the geometric properties, such as the height of specimen a, shear band thickness d and inclination angle α; (3) Determine the softening stiffness matrices D_{11} and D_{21}at post-localization by the relationships given in Eqs.39 and 40; (4) Obtain the incremental major principal stress $d\sigma_1$and incremental minor principal strain $d\varepsilon_3$; which are used further to determine the deviatoric stress on the stress surface and volumetric strain, respectively, by the relationships given in Eqs. 41 and 42. Incremental analysis was applied in the case of a biaxial compression with strain-softening elastoplasticity. In this particular case, incremental softening elastoplasticity was found to produce negative values in the tangential stiffness matrix D_{11}. Hence,

according to Eq. 41, this negative value will produce negative values for the incremental loading stress $d\sigma_1$. The development of the stress state σ_i can be regarded as an incremental process:

$$\sigma_i = \sigma_{i-1} + d\sigma_i \tag{43}$$

In this relation σ_i represents the actual state of stress and σ_{i-1}represents the previous state of stress, with its initial value at bifurcation point. The derivative $d\sigma_1$ is negative during softening.

After the maximum deviatoric stress q_{i-1} at the point of bifurcation is reached, the specimen enters the softening stage and the deviatoric starts to decrease.

$$q_i = \frac{1}{2}(\sigma_i - \sigma_3) \tag{44}$$

The first incremental loading point in the body of this model has been directly imposed at the end of the bifurcation point. The incremental loading used for this analysis did not include elastic and hardening loading which is already available in the hardening plasticity model developed by (Gutierrez 2010). The model developed herein is capable of describing the strain softening regime as well as identifying the stress state which corresponds to softening which is considered to coincide with the satisfaction of localization condition (Hill 1962; Rice 1976)

The softening constitutive model has been implemented into a spread sheet in an incremental form. The incremental form of the new softening model is provided in Eqs. 41 and 42 and can be used to calculate the elasto-plastic deformation. Data from biaxial compression testing on RH-Hostum sand and through DEM analysis for this sand has been selected to demonstrate the proposed softening model.

6. Model Demonstration

The following section intends to demonstrate strain softening through the use of the developed constitutive model. Model predictions are compared against DEM analysis and experimental data. The demonstration is performed for two densities (loose and dense) of RF-Hostun sand. In each of these demonstrations, data were taken from drained biaxial tests reported by [17]. RF-Hostun sand is fine grained; the mean particle diameter D_{50} is 0.35mm. Other sand properties and details are reported in *Desrues and Viggiani's strain localization in Sand: An Overview of Experimental Results Obtained in Grenoble Using Stereophotogrammetry*(2004). A demonstration will also be made for a DEM dense granular material, as performed by [18]. Comparisons will be made in terms of the predicted deviatoric stress-strain response from the softening elastoplasticity model

beyond bifurcation point. The stress-strain prediction will be demonstrated with the DEM and experimental data.

The plane strain biaxial test results for loose and dense RF-Hostun sands and DEM simulations were performed on samples isotropically consolidated at initial mean stresses of $S_0 = 200, 400\ and\ 800KPa$. The specimens were then sheared under constant stresses σ_3 and strain ε_1 control. The results are shown in Figs. 6, 7 and 8 for dense, loose RF-Hostun and DEM samples, respectively, in terms of deviatoric stress q vs. axial strain ε_1 and volumetric strainε_v vs. axial strainε_1 . The predicted results from the developed softening constitutive model are compared to each experimental and DEM sample. All granular samples, which were sheared at up to 10% of shear strains, exhibit well-defined peak shear stresses and dilatant responses at large strains. As can be seen in Fig. 6a, the relationship between deviatoric stress q and strain can show a clear strength softening behavior in the stress-strain curve, with sudden rate change from hardening to softening at the bifurcation point. This can be explained by a dramatic change in tangential stiffness matrix D_{11}immediately after the bifurcation point. The developed softening model accurately depicts this trend in the experimental data, as can be seen on Figure 6a. Figure 6b shows the relationship between volumetric and axial strain for dense RF-Hostun sand. It is clear that the developed softening model followed the trend of experimental data. Figure 7a show a gradual softening for loose RF-Hostun after the bifurcation point. In term of stress-strain curves, there may be a small difference in the tangential stiffness matrix D_{11} . Volumetric contraction is more pronounced for the loose sample than the dense sample as can be seen in Fig. 7b. The predicted results of softening model and experimental results are in good agreement for the two lower values of σ_3 and exhibit a slight divergence at the high value of σ_3 . Similarly, the constitutive model predicts the trend of softening behavior and shows good agreement with the DEM stress-strain curves.

The softening curves show contraction of the stress path beyond the bifurcation point as can be seen in Fig. 8a. All softening curves of the constitutive model have a similar philosophy, to give the tangent matrices an essential role, which is needed to define the softening behavior beyond bifurcation. The degree of softening is related directly to internal variables which therefore form the tangent matrix D_{11}. For example, the model assumes that the friction angle ϕ and dilation angle φ vary and depend on the stress level. The model also assumes that any calculation of strain softening should include a finite width for the strain localization zone. This is in close agreement with experimental data.

As can be seen in Figs. 6, 7 and 8, the post-localization strain softening is more pronounced in the dense samples than the loose samples and at high confining stresses than low confining stresses. Whereas, volume reduction is more pronounced for low confining stresses than high

confining stresses and for the loose samples than dense samples. Thus an analysis of softening curves for the constitutive model needs to represent both the material and geometric components of strain softening. With such analysis experimental test data could be interpreted objectively. It should then be possible to successfully predict the behavior of test specimens of various shapes and sizes. In order to give more attention to the geometric component of strain softening (refer to length scaleη), investigation will be conducted on the influence of this parameter on the response of strain softening.

7. The Influence of Length Scale η on Softening Elastoplasticity Model

The length scaleη, following the Pietruszczak and Mroz model [2]depends on thickness of shear band, specimen height a and the inclination of the shear band α as described in Eq. 5. In order to give more attention to the influence of the shear band thickness d on strain softening, the choice of the length scaleη will be conducted based on the variation of the values of d with keeping a and α constant. To further investigate the effect of the length scaleη on softening behavior, mathematical analyses have been carried out for$\eta = 0.0, 0.01, 0.05$ and 0.1, by keeping all other internal variables constant. All calculations presented here have been carried out with a confining stress σ_3 equals$800\ KPa$. The value $\eta = 0.0$ represents a shear band thickness equal to zero ($i.e.\ d = 0.0$). As the value of η increases the strain localization becomes wider

Figure 9 illustrates the prediction of the softening behavior using the softening elastoplasticity model. It shows that the length scale strongly influences the prediction of softening behavior. Shear bands can potentially have zero thickness at or beyond the bifurcation point, which effectively relates to zero softening. However, the analysis indicates that no localization is expected if the model includes a shear band with zero thickness. Length scale η serves to increase the shear band softening, giving rise to an interpretation of shear banding as a localization of strains resulting from internal variables associated with the tangential stiffness matrix D_{11}. It is observed that η or the width of localization zone d increases when the stiffness matrix D_{11} becomes more negative or the amount of softening is more dominated. The term softening implies that the increase in the length scale η causes a reduction in an incremental stress loading. For example, the use of a high η (0.1) induces an increase of the amount of softening. The thickness of shear band governs the degree of softening. The degree of softening is in this case is defined as the negative slope of the curve of deviatoric stress-strain.

8. Conclusion

The softening model predicts softening behavior using the constitutive stiffness matrices function, and is summarized as the follows:

1. It provides a realistic transition from hardening to softening at the bifurcation point. The abrupt transition observed in Fig. 6 indicates a sudden rate change from hardening to softening at the bifurcation point. On the other hand, Figure 7 shows the changing rate from soil hardening to softening is gradual and smooth. It indicates that stress state remain constant at a residual strength when soil experiences large strains, as show in Figs. 6, 7, and 8

2. It is based on the strain space elastoplasticity theory used to model granular soil behavior in the strain hardening model [1]and is then coupled with a strain softening model (the present work). The yield function describes the shape and the size of yield surface. The increasing and decreasing size of yield surface is controlled by hardening and softening respectively.

3. The behavior of elasto-plastic degradation is observed for granular soils in the post peak range. The major advantages of this model include strain softening and the residual state, so the model can predict a wide range of soil stress paths.

4. The model gives flexibility to fit a wide range of experimental data (loose and dense sand). The parameters used are shape factors, softening modulus B, and the shear band thickness$d$. These parameters can be further adjusted on the basis of experimental data.

5. The model can be modified to discuss strain softening under different boundary conditions, it is reasonable to generally use the plasticity theory.

6. The length scale parameter η, has non-dimensional length, which shows the effect of shear band thickness in the formulation of a softening model. The results show that increasing of strain localization thickness leads to increasing the amount of softening.

References

[1] Gutierrez, M.2010. Effects of constitutive parameters on strain localization in sands. *Int. j. Numer. Anal. Geomech.* 35(2): 161-178.

[2] Pietruszczak, S. and Mroz, Z. 1981. Finite Element Analysis of Deformation of Strain Softening Materials. Int. J. Num. Meth. Eng. **17**: 327-334.

[3] Nayak, G.C and Zienkiewicz, O.C.1972. Elasto-plastic stress analysis: a generalization for various constitutive relations including strain softening. Int. J. numer. Meth Engng. **5:** 113–135.

[4] Bazant. Z.P. 1988. Softening Instability: Part I — Localization into a Planar Band. Trans. ASME, J. Appl. Mech. **55**: 517.

[5] Rice, J.R. 1976. The Localization of Plastic Deformation, in Theoretical and Applied Mechanics, *Proceedings of the 14th International Congress on Theoretical and Applied Mechanics, Delft*, 1: 207-220.

[6] Rudnicki, J.W., and Rice, J.R. 1975. Conditions for the Localization of Deformation in Pressure-Sensitive Dilatant Materials, *Journal of the Mechanics and Physics of Solids*, 23: 371-394.

[7] Vermeer, P.A. 1982. A simple shear-band analysis using compliances. In: *IUTAM Conf.* on Deformation and Failure on Granular Materials, 439–499.

[8] Vardoulakis, I. and Sulem, J. 1995. Bifurcation Analysis in Geomechanics, *Blackie Academic and Professional*.

[9] Conte,*E.; Silvestri, F.; Troncone, A. 2010.* Stability analysis of slopes in soils with strain-softening behaviour. *Computers and Geotechnics*, 37(5):710-722.

[10] Wanatowski, D., Chu, J., Lo, R.C.2008. Strain-softening behavior of sand in strain path testing under plane-strain conditions · *ActaGeotechnica* 3: 99-114.

[11] Broja and Regueiro R.A. 2001. Strain localization of frictional materials, *Computer Methods in Applied Mechanics and Engineering*, 190:2555-2580.

[12] Prager W. 1956. A New Method of Analyzing Stresses and Strains in ... *ASME Journal of Applied Mechanics.*78: 493-496.

[13] Prager, W. 1949. Recent developments in the mathematical theory of plasticity. *J. appl. Phys.*20: 235.

[14] De Borst R., Sluys, L.J., Muhlhaus, H.B. and PAMIN, J. 1993. Fundamental issues in finite element analyses of localization of deformation. *Engineering Computations*, 10(2): 99-121.

[15] Schaeffer, David G.1990. *Instability and ill-posedness in the deformation of granular materials,Int. J. Numer. Anal. Methods Geomech*. 14(4): 253-278.

[16] De Borst R, Muhlhaus H. B.1992. Gradient-dependent plasticity: Formulation and algorithmic aspects. *Int. J. Numer. Methods Eng.* 35:521-539.

[17] Desrues J, Hammad W. 1989. Experimental study of the localization of deformation on sand: influence of mean stress. *Proceedings of the 12th International Conference on Soil Mechanics and Foundation Engineering*, Rio de Janeiro 1: 31-32.

[18] Mohamed, A., and Gutierrez, M. 2010. Comprehensive study of the effects of rolling resistance on the stress–strain and strain localization behavior of granular materials, Gran. Matter **12** (5): 527–541.

[19] Desrues J, Viggiani G.2004. Strain localization in sand: an overview of expertimental results obtained in Grenoble using stereo photogrammetry. *International Journal for Numerical and Analytical Methods in Geomechanics*28: 231–279.

[20] Bazant, ZP, and Chang, TP. 1987. Nonlocal Finite Element Analysis of Strain- Softening Solids," *J. Struct. Eng. (ASCE)*, 113(1):89-105.

[21] Belytschko, T., and Mish, K. 2001. Computability in non-linear solid mechanics, *International Journal for Numerical Methods in Engineering*, 52 (1-2):3.

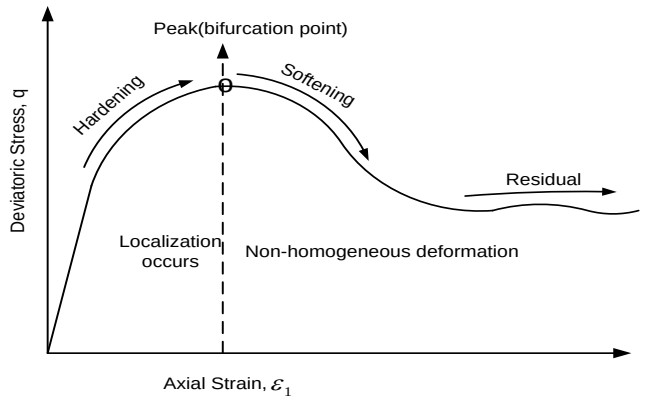

Figure 1 Typical deviatoric stresses vs. axial strain behavior of frictional soil

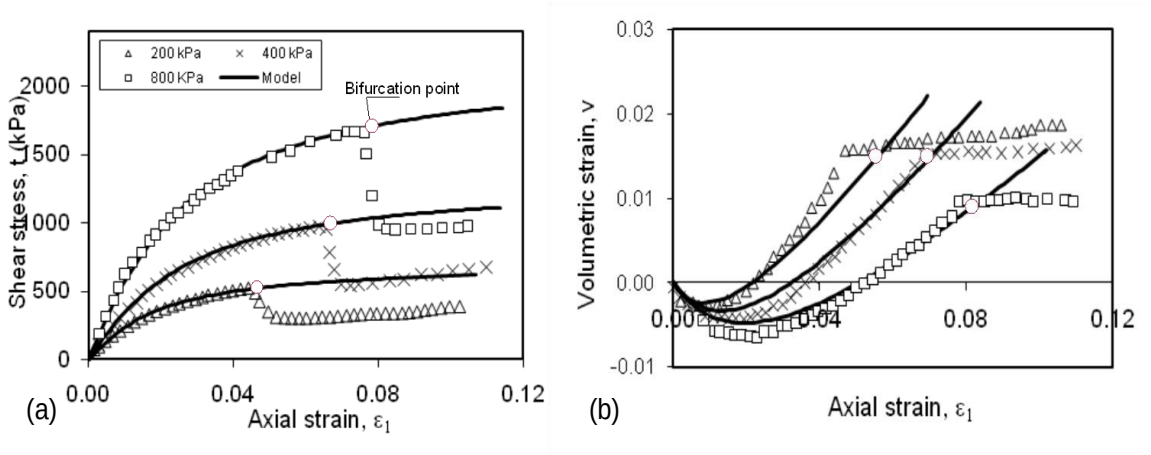

Figure 2 Comparison between Hardening Model (Gutierrez 2010) and experimental data for dense RF-Hostum sand under plane strain biaxial tests. Values shown in the legend are the confining stress used in each tests. (a) Shear stress vs. axial strain. (b) Volumetric strain vs. axial strain.

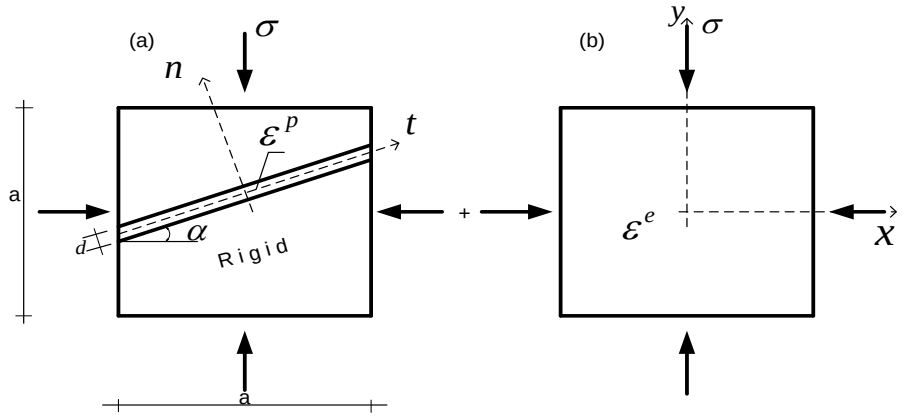

Figure 3 The mode of deformation of a representative element (Pietruszczak and Mroz 1981).

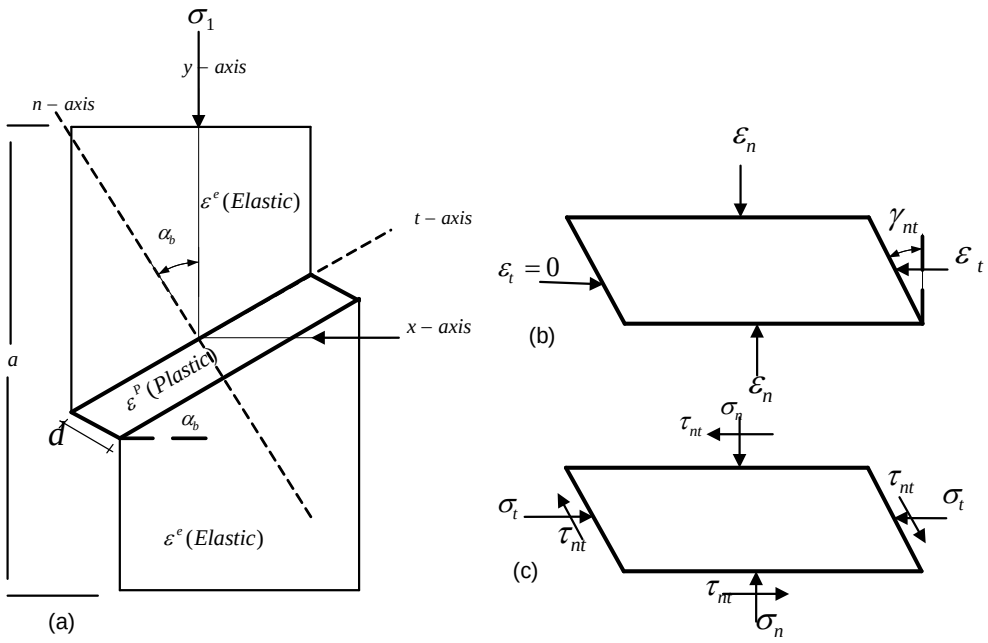

Figure 4 (a) Idealized shear band geometry in the biaxial test, (b) Applying principal strains and (c) Applying principal stresses.

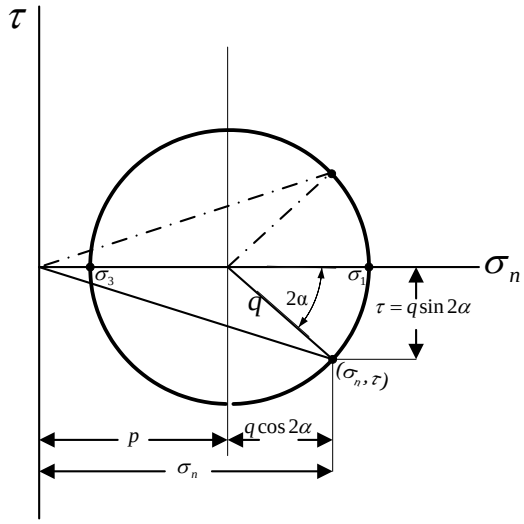

Figure 5 Relationship between principal stresses and the stresses in the shear band

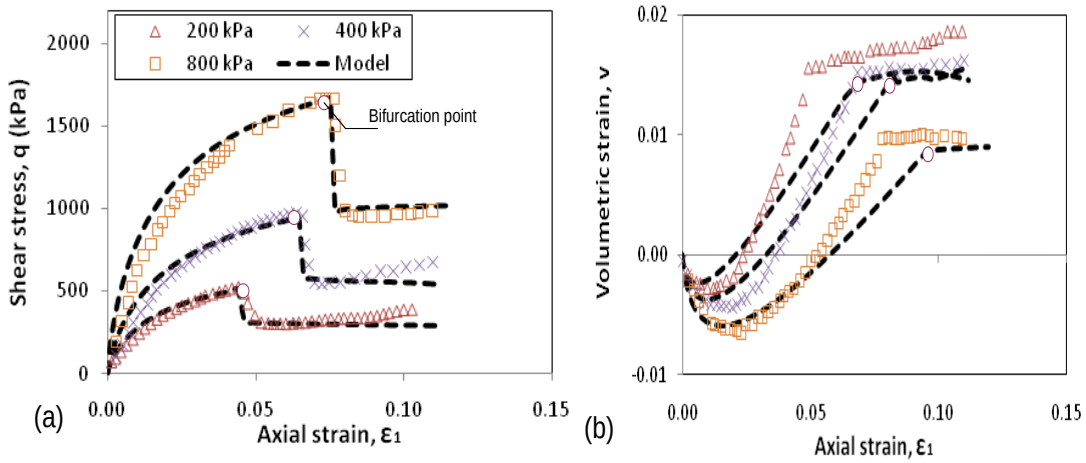

Figure 6 Comparison between Post-bifurcation Model and experimental data for dense RF-Hostum sand under plane strain biaxial tests. Values shown in the legend are the confining stress used in each tests. (a) Shear stress vs. axial strain. (b) Volumetric strain vs. axial strain.

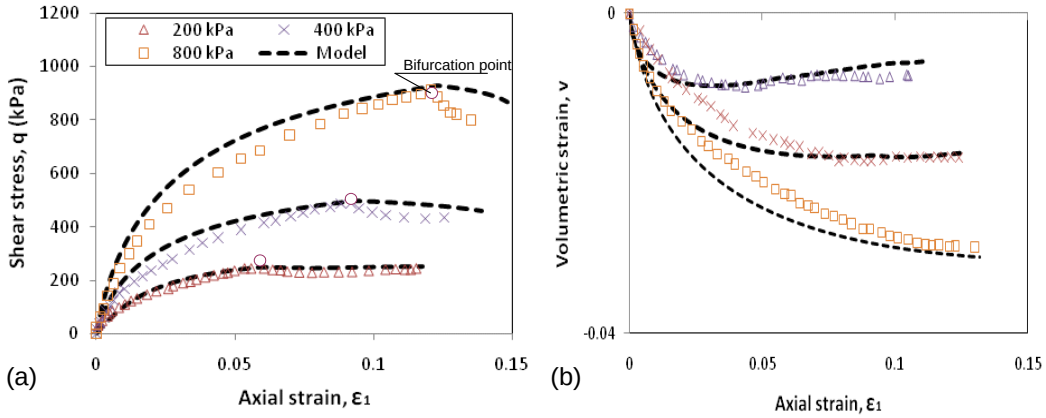

Figure 7 Comparison between Post-bifurcation Model and experimental data for loose RF-Hostum sand under plane strain biaxial tests. Values shown in the legend are the confining stress used in each tests. (a) Shear stress vs. axial strain. (b) Volumetric strain vs. axial strain.

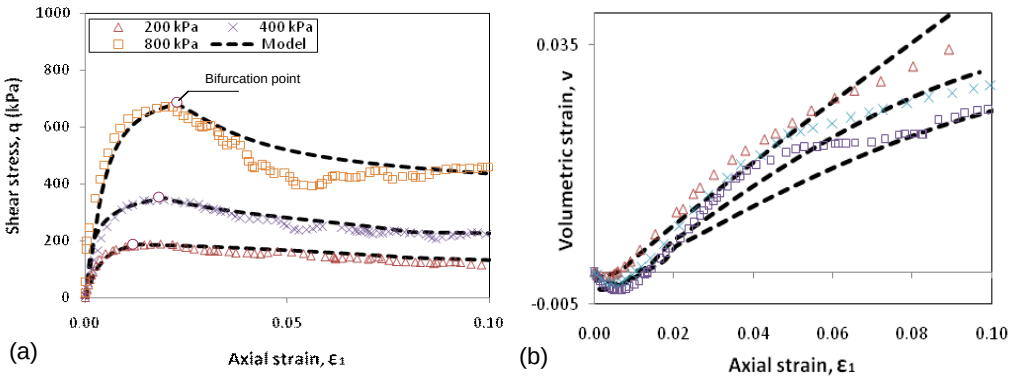

Figure 8 Comparison between Post-bifurcation Model and DEM data for dense Particles under plane strain biaxial tests. Values shown in the legend are the confining stress used in each tests. (a) Shear stress vs. axial strain. (b) Volumetric strain vs. axial strain.

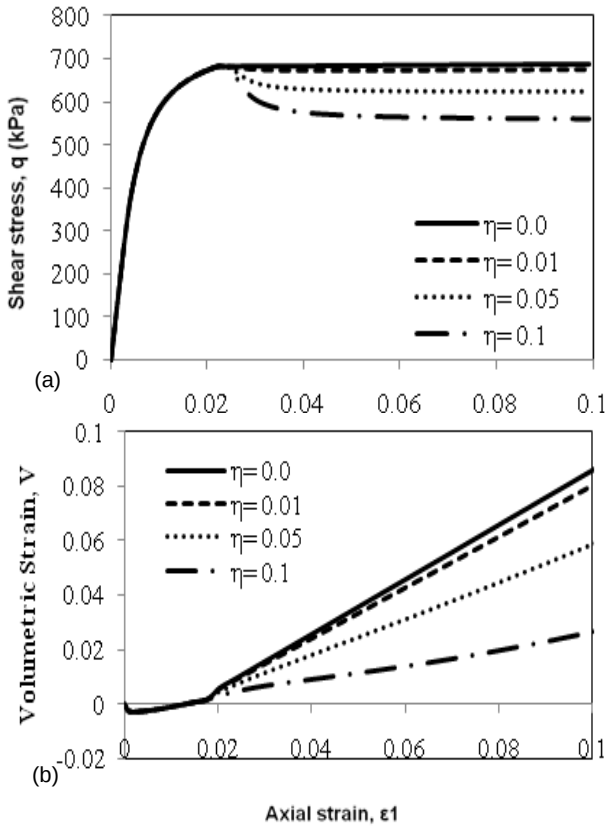

Figure 9 The influence of Length Scale η on Softening Elastoplasticity Model (a) Stress-strain curves (b) Volumetric strain-strain.